
Since January 2020 Elsevier has created a COVID-19 resource centre with free information in English and Mandarin on the novel coronavirus COVID-19. The COVID-19 resource centre is hosted on Elsevier Connect, the company's public news and information website.

Environmental Pollution 289 (2021) 117899

Contents lists available at ScienceDirect

Environmental Pollution

journal homepage: www.elsevier.com/locate/envpol

# Opposite impact of emission reduction during the COVID-19 lockdown period on the surface concentrations of $PM_{2.5}$ and $O_3$ in Wuhan, China☆

Hao Yin [a,b], Cheng Liu [a,b,c,d,e,*], Qihou Hu [a], Ting Liu [g], Shuntian Wang [a,b], Meng Gao [f], Shiqi Xu [g], Chengxin Zhang [b], Wenjing Su [g]

[a] Key Laboratory of Environmental Optics and Technology, Anhui Institute of Optics and Fine Mechanics, HFIPS, Chinese Academy of Sciences, Hefei, 230031, China
[b] Department of Precision Machinery and Precision Instrumentation, University of Science and Technology of China, Hefei, 230026, China
[c] Center for Excellence in Regional Atmospheric Environment, Institute of Urban Environment, Chinese Academy of Sciences, Xiamen, 361021, China
[d] Key Laboratory of Precision Scientific Instrumentation of Anhui Higher Education Institutes, University of Science and Technology of China, Hefei, 230026, China
[e] Anhui Province Key Laboratory of Polar Environment and Global Change, University of Science and Technology of China, Hefei, 230026, China
[f] Department of Geography, Hong Kong Baptist University, Kowloon Tong, Hong Kong SAR, China
[g] School of Earth and Space Sciences, University of Science and Technology of China, Hefei, 230026, China

ARTICLE INFO

*Keywords:*
Generalized additive models
Meteorological factors influence
Atmospheric pollution
Titration effect
VOC reduction

ABSTRACT

To prevent the spread of the COVID-19 epidemic, the Chinese megacity Wuhan has taken emergent lockdown measures starting on January 23, 2020. This provided a natural experiment to investigate the response of air quality to such emission reductions. Here, we decoupled the influence of meteorological and non-meteorological factors on main air pollutants using generalized additive models (GAMs), driven by data from the China National Environmental Monitoring Center (CNEMC) network. During the lockdown period (Jan. 23 – Apr. 8, 2020), $PM_{2.5}$, $PM_{10}$, $NO_2$, $SO_2$, and CO concentrations decreased significantly by 45 %, 49 %, 56 %, 39 %, and 18 % compared with the corresponding period in 2015–2019, with contributions by S(meteos) of 15 %, 17 %, 13 %, 10 %, and 6 %. This indicates an emission reduction of $NO_x$ at least 43 %. However, $O_3$ increased by 43 % with a contribution by S(meteos) of 6 %. In spite of the reduced volatile organic compound (VOC) emissions by 30 % during the strict lockdown period (Jan. 23 – Feb. 14, 2020), which likely reduced the production of $O_3$, $O_3$ concentrations increased due to a weakening of the titration effect of NO. Our results suggest that conventional emission reduction ($NO_x$ reduction only) measures may not be sufficient to reduce (or even lead to an increase of) surface $O_3$ concentrations, even if reaching the limit, and VOC-specific measures should also be taken.

## 1. Introduction

With the rapid development of China, the air quality problem in this country has gradually become more serious in this century (Yin et al., 2019). To prevent and control air pollution, the Chinese government has taken many measures to reduce anthropogenic emissions, such as the Air Pollution Prevention and Control Action Plan issued in September 2013 (Chinese Government, 2013). With the implementation of these measures, air quality in China has greatly been improved (Vu et al., 2019; Zhang et al., 2019b). The number of severe haze pollution days in Beijing–Tianjin–Hebei (BTH) and the Changjiang River Delta (YRD) areas decreased from 122 to 33 in 2013 to 31 and 25 in 2017, respectively (Li et al., 2019a). Air quality can be affected not only by anthropogenic emissions but also by meteorological conditions (Han et al., 2020; Yin et al., 2021; Yin et al., 2020). For instance, a higher planetary boundary layer height (PBLH) is propitious to the disappearing of air pollutants (Li et al., 2017a; Su et al., 2018). Meteorological factors in winter are more unfavorable to diffusion and dilution of pollutants and cause the accumulation of more pollutants at the surface (Yang et al., 2019). The importance of meteorological conditions in controlling ozone ($O_3$) pollution was described by Han et al. (2020). Ansari et al. (2019) demonstrated that under unfavorable meteorological conditions, the same reduction emission measurements as under favorable conditions would not achieve satisfactory effects for fine particulate matter (PM).

☆ This paper has been recommended for acceptance by Da Chen.

* Corresponding author. Key Laboratory of Environmental Optics and Technology, Anhui Institute of Optics and Fine Mechanics, HFIPS, Chinese Academy of Sciences, Hefei, 230031, China.
*E-mail address:* chliu81@ustc.edu.cn (C. Liu).

https://doi.org/10.1016/j.envpol.2021.117899
Received 4 May 2021; Received in revised form 26 July 2021; Accepted 1 August 2021
Available online 2 August 2021

Because of the complicated non-linear relationship between meteorological conditions and air quality, it is still a challenge to separate the influence of emissions and meteorological factors on air quality (Zhang et al., 2019a; Zhong et al., 2018). In one of our previous studies, the generalized additive models (GAMs) model was employed to quantify the contribution of meteorology and anthropogenic emissions to the variation in the concentrations of tropospheric nitrogen dioxide ($NO_2$), sulfur dioxide ($SO_2$), and formaldehyde (HCHO) in four megacities in China, i.e., Beijing, Shanghai, Guangzhou, and Chengdu (Zhang et al., 2019a).

During many important social events, such as the Beijing Olympic Games in 2008, the Beijing APEC conference in 2014, the Grand Military Parade in Beijing 2015 as well as the Youth Olympic Games in 2014 in Nanjing and the G20 conference in 2016 in Hangzhou, anthropogenic emissions reduced greatly through a strict temporary emission control (Gao et al., 2016; Huang et al., 2017; Li et al., 2017c; Liang et al., 2017; Su et al., 2017). Such events provide a natural laboratory to assess the impact of emission reduction and meteorology on air pollution. For instance, during the Sino-African Summit in Nov. 4–6, 2006, traffic restrictions induced a reduction in particle number concentrations in Aitken and accumulation modes at the ground by 20%–60 % and a reduction of the vertical column density (VCD) of $NO_2$ by 40 % (Cheng et al., 2008; Wang et al., 2007). Gao et al. (2011) concluded that emission control and favorable meteorological conditions together induced the decrease of aerosol species by 30–50 % during the Olympic period, while emission control was the dominant factor. Huang et al. (2017) found that emission reduction had a dominant influence on the improvement in air quality during the Nanjing Youth Olympic Games in spite of unfavorable meteorological conditions. Using a generalized linear regression model, Liang et al. (2017) found that emission control and meteorological conditions contributed to a 30 % and 28 % decrease in $PM_{2.5}$ concentrations during the APEC conference, respectively, and a 38 % and 25 % decrease during the China Victory Day Parade 2015, respectively. However, during the G20 conference, temporary measures took no immediate effect on controlling $O_3$ pollution in the boundary layer, while meteorological conditions dominated the variation of $O_3$, although $PM_{2.5}$ concentrations decreased significantly (Su et al., 2017). Li et al. (2017c) reported that the of $PM_{2.5}$ concentrations predicted by the Weather Research and Forecast and Community Multi-scale Air Quality (WRF-CMAQ) model were reduced by 56 % due to reduction emission measurements.

The Corona Virus Disease 2019 (COVID-19) is a serious infectious disease that had spread all over the world by March 2020. Up to April 30, 2021, the virus had caused more than 3 million deaths worldwide (World Health Organization, 2021). To prevent the spread of the epidemic, the city of Wuhan in China adopted the measures of shutting down local enterprises and restricting traffic transport (referred to as "lockdown") as the first city in the world to reduce the gathering of people. Wuhan has a permanent resident population of 11.212 million (Wuhan Government, 2021) and has suffered from air pollution in recent years (Shi and Brasseur, 2020b). During the lockdown period, the emission of air pollutants, except from residences, almost ceased, which may have abruptly changed the concentrations of air pollutants in Wuhan. Bauwens et al. (2020) evaluated the column of $NO_2$ over China via TROPOMI and OMI satellite data and reported a decrease by 40 % during the COVID-19 lockdown period compared with the corresponding period in 2019. However, there is still lack of an effective assessment of the influence of meteorological factors and emissions for this phenomenon. Shi et al. (Shi and Brasseur, 2020a) found a large increasing variation of $O_3$ by 35%–95 % in Wuhan during the COVID-19 outbreak, and attributed this increase to the decrease of $NO_x$ because during winter, $O_3$ is in volatile organic compound (VOC)-limited conditions and the production of $O_3$ is inversely related to that of $NO_x$. Wang et al. (2020) also reported that compared to the same period in 2019, concentrations of $PM_{2.5}$, $PM_{10}$, $SO_2$, $NO_2$, and CO in Hangzhou decreased by 42.7 %, 47.9 %, 28.6 %, 22.3 %, and 58.4 %, respectively, during the COVID-19 lockdown period, but $O_3$ increased by approximately 50 %. Le et al. (2020) investigated the causes of haze pollution by WRF-Chem during the COVID-19 lockdown period in the North China Plain. Not only in China, but also in Southeast Asia, where pollutant concentrations have fallen significantly due to lockdown in response to COVID-19 (Roy et al., 2021). However, due to the lack of VOCs data, the investigation on the causes of this phenomenon was not conclusive. In this paper, we aim to separate the effect of a change in anthropogenic emissions on the variation of air quality in Wuhan due to the lockdown measures from that of meteorological conditions. The concentrations of main air pollutants at the surface from the China National Environmental Monitoring Center (CNEMC) network and the tropospheric vertical column densities (VCDs) of HCHO from satellite-based remote sensing data were used to analyze the variation in air pollutants during the lockdown period in Wuhan. GAMs were adopted to single out the change in concentrations of different air pollutants induced by the anthropogenic emission reduction in Wuhan due to the lockdown measures from the influence of meteorological conditions. Our study provides useful insights into the role of extreme emission reduction measures in the improvement of air quality.

## 2. Methods

### 2.1. Data from the CNEMC network

The CNEMC network provides hourly records of the concentrations of $PM_{2.5}$, $PM_{10}$, $NO_2$, $SO_2$, CO, and $O_3$ all over China (http://www.cnemc.cn/en/, last access: 10 May 2020). The dataset has been widely used in numerous air quality studies (Li et al., 2018; Li et al., 2019b; Lu et al., 2019a; Meng et al., 2018; Shen et al., 2019). In this study, data of Wuhan from January 2015 to April 2020 were adopted. We applied a data quality control method, similar to that used in previous studies, to remove error data (Canton et al., 2015; Lu et al., 2018). Hourly observed datapoints were transformed into Z scores, and then, the observed data were removed if the corresponding $Z_i$ met one of the following conditions: (1) $Z_i$ is larger or smaller than the previous one ($Z_{i-1}$) by 9 ($|Z_i - Z_{i-1}| > 9$), (2) The absolute value of $Z_i$ is greater than 4 ($|Z_i| > 4$), or (3) the ratio of the Z value to the third-order center moving average is greater than 2 $\left(\frac{3Z_i}{Z_{i-1}+Z_i+Z_{i+1}} > 2\right)$. The formula for calculating $Z_i$ is as follows:

$$Z_i = \frac{X_i - \overline{X}}{\sigma} \quad (1)$$

where $X_i$ represent the i-th item in the dataset, and $\overline{X}$ and $\sigma$ are the average and standard deviation of dataset X, respectively. The distribution of CNMEC sites in Wuhan is shown in Fig. S1.

### 2.2. TROPOspheric monitoring instrument (TROPOMI) data

Tropospheric VCDs of HCHO and $NO_2$ were retrieved from the TROPOMI satellite spectrum to trace the variation of VOCs and study the spatial distribution of emission reductions (Su et al., 2020; Veefkind et al., 2012). TROPOMI is a satellite instrument on board the Copernicus Sentinel-5 Precursor satellite. The Sentinel-5 Precursor (S5P) is the first of the atmospheric composition Sentinels, launched on October 13, 2017, planned for a mission of seven years. TROPOMI has four two-dimensional spectrometers with wavelengths from 270 to 2385 nm. The third band is from 320 to 405 nm for HCHO retrieval. The spectral resolution of this band is about 0.5 nm (half height and width). The spatial resolution of the instrument is 3.5 × 7 $km^2$ (Su et al., 2020). Details of the S5P operational HCHO algorithm can be found in (Smedt et al., 2018). The quality indicators for our TROPOMI products were as follows: (a) Root mean square (RMS) values of the spectral fit residual smaller than $10^{-3}$. (b) Cloud fraction (CF) < 0.3. (c) Air-Mass Factor

(AMF) > 0.1. (d) SZA (Solar zenith angle) < 70°. (e) Quality assurance (QA) > 0.55.

### 2.3. GAMs model

To separate the contribution of meteorological factors to air quality from other factors, we applied a statistical fitting method based on the GAMs model (Wood Simon, 2004). The GAMs model uses penalized smoothing splines to evaluate the influence of meteorological factors and anthropogenic emissions on the variation of air quality. The GAMs model uses a nonparametric smooth function, which can be a smooth spline function, a kernel function, or a local regression smooth function. Its nonparametric form makes the model very flexible, so that it can well reveal the nonlinear effect of independent variables. Pearce et al. (2011) estimated the responses of air pollutants, like $O_3$, $PM_{10}$, and $NO_2$, to meteorological parameters such as temperature, water vapor pressure, and others through the GAMs model. Otero et al. (2020) investigated the effect of $NO_x$ reductions in the $O_3$-temperature relationship using GAMs and found that the reduction of $NO_x$ was not the only factor causing variation in meteorology. In our previous study, GAMs was successfully applied to distinguish the contribution of meteorological and non-meteorological factors to pollutant concentrations, and the non-meteorological factors were verified to indicated emissions through comparison with the Multi-resolution Emission Inventory for China (MEIC) (Zhang et al., 2019a). The smoothing function was developed by combining model selection with automatic smoothing parameter selection using penalty regression splines, which were optimized to minimize dimensions in the model (Pearce et al., 2011). The selection of smoothing parameters was carried out by limiting the maximum likelihood (REML), and the confidence interval was estimated using the unconditional Bayesian method (Pearce et al., 2011). The fitting equation of the GAMs model can be written as follows(De Veaux, 2012):

$$\log(y) \sim \beta + \sum_{i}^{n} S(X_i) + \varepsilon \quad (2)$$

where y is the daily-averaged concentrations of air pollutants, $\beta$ is the constant mean of the response, $S(X_i)$ is the smoothing function term of the i-th component of n total covariates, and $\varepsilon$ is the residual of fitting. The covariates included meteorological factors and other temporal variables, including the day number (daynum) and the day of the week (dow), to consider the short-term temporal persistence and control for temporal autocorrelation in the residuals. The meteorological parameters included zonal (east-west) wind (ua), meridional (north-south) wind (va), relative humidity (RH), downward shortwave solar radiation at the surface (swdown), planetary boundary layer height (pblh), and temperature (temp) at the surface. The meteorological parameters were extracted from National Centers for Environmental Prediction (NCEP) Final Operational Global Analysis (FNL) datasets and simulated using the Weather Research and Forecasting (WRF) model with the horizontal resolution of 0.1°. In this study, we divided the dataset from 2015 to 2020 into a testing dataset and a training dataset, in which the training dataset accounted for 80 % and the testing set for 20 %. Data for 2020, were divided into the testing dataset.

## 3. Results

### 3.1. Validation of the GAMs model

The GAMs fitting results showed reasonably good agreement with the daily-average CNEMC-measured data for each pollutant from January 2015 to March 2020. The Pearson correlation coefficients (R) with the training dataset were 0.64, 0.68, 0.79, 0.76, 0.81, and 0.55 for $PM_{2.5}$, $PM_{10}$, $NO_2$, $SO_2$, $O_3$, and CO, respectively (Fig. S1). Moreover, the correlations with the testing dataset were 0.64, 0.67, 0.79, 0.77, 0.81, 0.55 for $PM_{2.5}$, $PM_{10}$, $NO_2$, $SO_2$, $O_3$, and CO, respectively (Fig. S2). In particular, correlation for all datasets in 2020 of 0.64, 0.67, 0.79, 0.77, 0.81, and 0.55 for $PM_{2.5}$, $PM_{10}$, $NO_2$, $SO_2$, $O_3$, and CO, respectively (Fig. S3). We also carried on several groups of different species for cross validation, including $NO_2$ and CO, $NO_2$ and $SO_2$, $SO_2$ and CO, and $PM_{2.5}$ and $PM_{10}$. These had high correlations of 0.75, 0.65, 0.91, and 0.82 (Fig. S4). The reason for choosing these groups for cross validation was that these pollutants have similar sources. Although this method does not include physical and chemical processes, the results well reproduced the variations in the measured air pollutants. The uncertainty of GAMs fitting did not exceed that of the statistical model used in other studies, such as Liang et al. (2017) (Table S1). The results for non-meteorological factors reflect well the decreasing trend of pollutant emissions in China in recent years (Fig. 1, Figure S5-S8 and S10).

### 3.2. Marginal effect of individual variables on air pollutants

To explain the impact of individual factors on air pollutants, we used the effect of the smooth term $S(X_i)$ in GAMs, calculated as $100\,\% \cdot [e^{S(X_i)} - 1]$, which represents the relative effect of an individual term to the total factor, where $X_i$ is the individual factor, and $S(X_i)$ represents the influence of each meteorological factor $X_i$ on pollutant concentration (Figs. 1, 2, and S12-15). The estimated degrees of freedoms (EDFs), which show the linear or nonlinear degree of fitting, corresponding to the individual terms are noted in each figure. An EDFs of 1 indicates a linear effect.

The influence of temperature on pollutants (S(temp)) was generally similar, except for $O_3$. Assuming that other influencing factors remain constant, the concentrations of pollutants except for $O_3$ rose by ~20 % as compared with the average values in 2015–2019, when the air temperature was below 10 °C (Fig. 2 (e)). With an increase in temperature, the formation of secondary sulfate would be enhanced due to the acceleration of the $SO_2$ oxidation rate (Jacob and Winner, 2009; Tai et al., 2010). For $NO_2$ and $SO_2$, this phenomenon may be partly explained by the accelerated evaporative emission rate of $NO_x$ and $SO_2$ at higher temperature (Pearce et al., 2011) (Figs. S13 and S14 (e)). When the air temperature was higher than 10 °C, pollutant concentrations decreased. For $O_3$, the influence of temperature was opposite to that of other pollutants. When the air temperature was higher than 15 °C, the concentration of $O_3$ strongly increased as compared with the average value in 2015–2019, as the reaction rate of the photochemical formation of $O_3$ is positively related with temperature (Ordonez et al., 2005); however, when temperature was below 15 °C, the concentration of $O_3$ decreased. Tropospheric $O_3$ is mainly produced by photochemical reactions of nitrogen oxidation ($NO_x$ = NO + $NO_2$) and VOCs (Jacob and Winner, 2009; Lu et al., 2019b). Temperature can also affect $O_3$ formation through altering the emission of precursors. At high temperature, both biological and evaporative emissions of anthropogenic VOCs were increased (Jacob and Winner, 2009; Ordonez et al., 2005). A similar effect of meteorological conditions on air pollutants has been reported by some studies (Neftel et al., 2002; Weber and Prevot, 2002).

The influence of relative humidity (RH) on $PM_{2.5}$ was positive in the range of less than 60 % (Fig. S1 (c)). When RH is high, heterogeneous reactions and the formation of secondary aerosols can accelerate with an increase in water vapor in the ambient air (Pendergrass et al., 2019; Wang et al., 2016; Zhang et al., 2020; Zheng et al., 2015), causing higher $PM_{2.5}$ masse concentrations. However, in the range of 60%–80 %, the influence of RH on increasing $PM_{2.5}$ masse concentrations weakened. RH is generally negatively correlated with $PM_{10}$, $NO_2$, $SO_2$, and $O_3$ (Jacob and Winner, 2009)(Fig. 2 (c) and Figs. S12–14 (c)). Due to the fact that $PM_{10}$ is mainly composed of coarse particles and originates from primary emissions, a higher RH may accelerate the settlement and removal of $PM_{10}$ (Leung et al., 2018; Zhu et al., 2012). Because OH radicals consume $NO_2$, $SO_2$ in the troposphere, and the reaction of water vapor with $O(^1D)$ atoms is the main source of OH radicals, RH showed a negative influence on the concentrations of $NO_2$, $SO_2$ (Atkinson, 2000; Johnson et al., 1999). In addition, humidity increases the heterogeneous conversion of $NO_2$ and NO to $HNO_3$ and $SO_2$ to $H_2SO_4$ (Khoder, 2002;

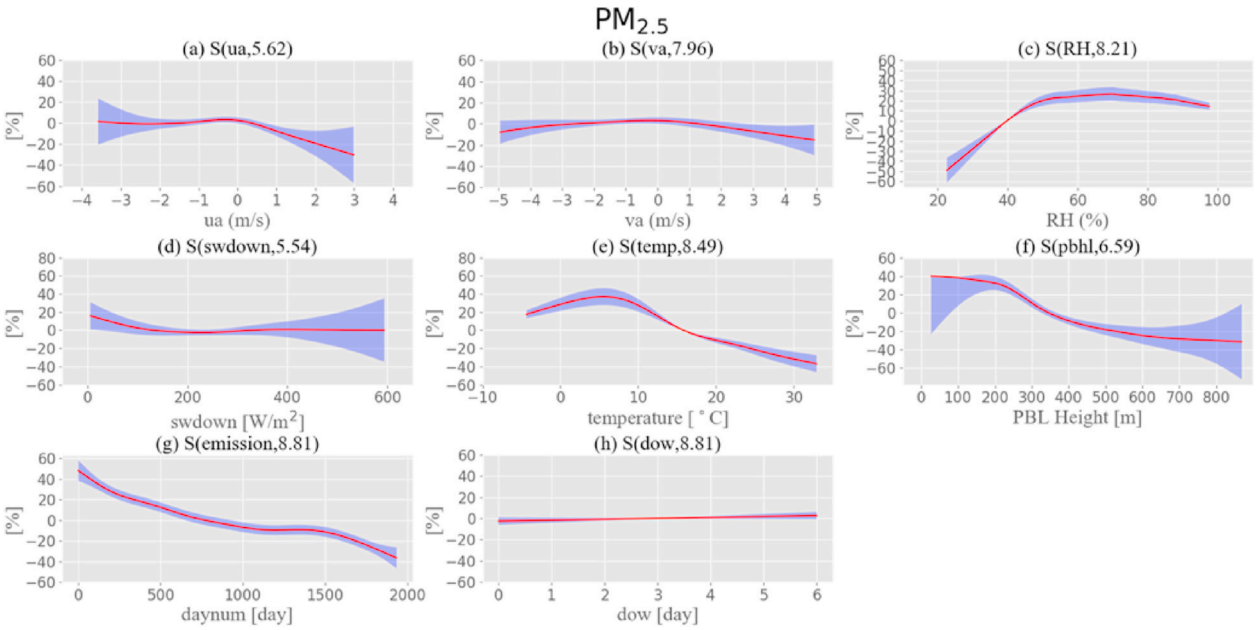


**Fig. 1.** The effects of each individual meteorological variable in the GAM model on hourly $PM_{2.5}$ in Wuhan. (a)–(f) variables of zonal wind (ua), meridional wind (va), relative humidity (RH), downward shortwave solar radiation at the surface (swdown), temperature (temp) and planetary boundary layer height (pblh) are presented in these plots.

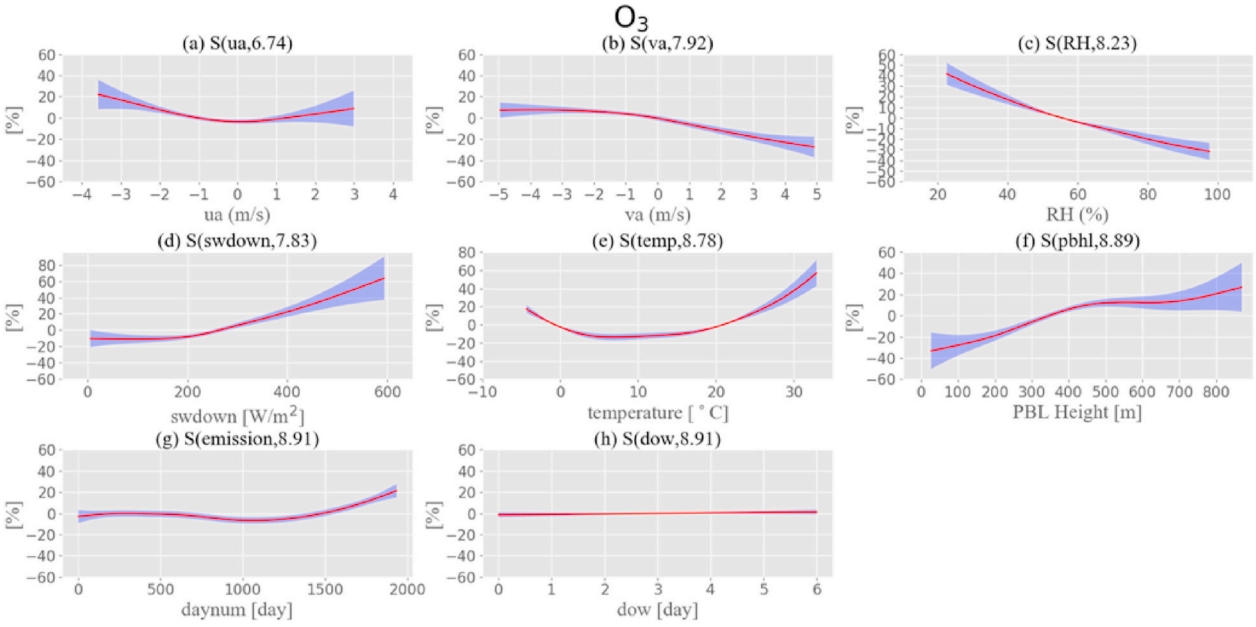


**Fig. 2.** The effects of each individual meteorological variable in the GAM model on hourly $O_3$ in Wuhan. (a)–(f) variables of zonal wind (ua), meridional wind (va), relative humidity (RH), downward shortwave solar radiation at the surface (swdown), temperature (temp) and planetary boundary layer height (pblh) are presented in these plots.

Kleffmann and Wiesen, 2005). This reason is also responsible for the negative correlation between RH and $O_3$, but some studies found that this occurs mainly in remote regions, and even enhances ozone production in high $NO_x$ regions (Sillman et al., 1990). Other factors also include: (1) the correlation of humid days with increased cloud and reduced photochemistry (Xu et al., 2011). (2) the association of wet days with rainout and reducing precursor emissions (Elminir, 2005). (3) the greater susceptibility to stratospheric intrusion in dry weather (Jiang et al., 2015). In Wuhan, during 2015–2019, $O_3$ concentrations under dry days were on average 22%–50 % higher per year than under humid days (Fig. S16). RH increased the concentrations of CO, but with an increase in RH, the increasing trend slowed down, and even a slight decrease in concentration occurred when RH > 60 % (Fig. S15 (c)).

The planetary boundary layer height (PBLH) showed a negative correlation with $PM_{2.5}$, $PM_{10}$, $NO_2$, $SO_2$, and CO concentrations but a positive correlation with $O_3$. The primary emission or secondary formation of $PM_{2.5}$, $PM_{10}$, $NO_2$, $SO_2$, and CO mainly occurs at the surface. However, $O_3$ concentrations in the upper boundary layer are usually higher than those in the lower boundary layer (Su et al., 2017; Zhao et al., 2019), so that a higher boundary layer height is conducive to the downward transport of $O_3$ from the upper layer. Therefore, for an increase of the PBLH from 0 m to 1000 m, the concentrations of $PM_{2.5}$,

$PM_{10}$, $NO_2$, $SO_2$, and CO would decrease by about 40%–80 % of their average values in 2015–2020 (Fig. 1 (f), Figs. S12–S15 (f)), respectively; however, $O_3$ concentrations would increase by about 60 % of their average value (Fig. 2 (f)).

There was an increasing effect between $O_3$ and downward shortwave solar radiation (swdown) (Fig. 2 (d)). Higher levels of swdown at the surface could promote the elevation of $O_3$ because intense radiation would lead to the enhancement of photochemical reactions producing $O_3$ (Lacis and Hansen, 1974). Swdown had a slight influence on $PM_{2.5}$, $PM_{10}$, and CO, and a negative influence on $NO_2$ and $SO_2$ concentrations (Fig. 1 (d), Figs. S12–S15 (d)).

The influence of zonal wind on pollutants was consistent. The positive values of ua represent easterly winds and negative values represent westerly winds, while the positive value of va represents the north wind and the negative value represents the south wind. For particulate matter, the eastern winds led to a large decrease in $PM_{2.5}$ and $PM_{10}$ concentrations. The concentration of CO is affected more similarly to the particulate matter. The south and east winds caused a large decrease in $NO_2$ and $SO_2$ concentrations. For $O_3$, east, west and south wind increased concentrations, while north wind decreased concentrations (Fig. 2 (a) and (b)). Other meteorological factors also had a slight impact on air pollutants, but the impact range was not obvious in the specific analysis above.

From the marginal effect of S(dow), we conclude that there was no weekly variation cycle in Wuhan. According to our previous study, the contribution of the day number (daynum) for primary pollutants like $NO_2$, $SO_2$, represented the influence of emissions(Zhang et al., 2019a). However, for air pollutants which contain secondary components like $O_3$, $PM_{2.5}$, and $PM_{10}$, S(daynum) may not only represent the influence of emissions, but also of chemical reactions.

The contribution of meteorological factors (s(meteos), the amount of pollutant change due to meteorological factors) and non-meteorological factors (s(non-meteos), the amount of pollutant change due to non-meteorological factors, i.e., temporal terms), on air pollutants were calculated as the sum of the contributions of individual factors. In general, s(non-meteos) can be considered an indicator of anthropogenic emissions to some extent (Zhang et al., 2019a). Similar to our previous study, meteorological factors dominated day-to-day variation with Pearson correlation coefficients of 0.63–0.82 for the observed pollutants (Fig. 3); however, on the interannual scale, the variations of air pollutant concentrations were determined by non-meteorological factors. From 2015 to 2019, concentrations of $PM_{2.5}$, $PM_{10}$, $NO_2$, $SO_2$, and CO in Wuhan decreased by 23 μg/m$^3$, 32 μg/m$^3$, 6 μg/m$^3$, 8 μg/m$^3$, and 0.1 mg/m$^3$, respectively, while those of $O_3$ increased by 5 μg/m$^3$. S (non-meteos) for $PM_{2.5}$, $PM_{10}$, $NO_2$, $SO_2$, and CO also decreased by 26 μg/m$^3$, 43 μg/m$^3$, 10 μg/m$^3$, 9 μg/m$^3$, and 0.1 mg/m$^3$ compared with 2015 and 2019, respectively. However, S(non-meteos) had positively contributed to $O_3$ concentrations, which increased by 5 μg/m$^3$. S (meteos) for $PM_{2.5}$, $PM_{10}$, $NO_2$, $SO_2$, $O_3$, and CO increased by 4 μg/m$^3$, 5 μg/m$^3$, 2 μg/m$^3$, 1 μg/m$^3$, 1 μg/m$^3$, and 0.01 mg/m$^3$ compared with 2015 and 2019, respectively (Fig. 4).

### 3.3. Variation of particulate matter during the lockdown period

To investigate the influence of the control measures on air quality in Wuhan, we compared air quality in different control stages: I. pre-lockdown stage (Jan. 1 – Jan. 22, 2020), during which anthropogenic activities went on as usual; II. lockdown stage (Jan. 23 – April 8, 2020), including the strict-lockdown (Jan. 23 – Feb. 14) period, during which prohibited almost all anthropogenic polluting activities, and the slight-lockdown stage (Feb. 15 – April 8, 2020), during which some enterprises in Wuhan gradually returned to work, but civilian traffic in Wuhan still suspended; III. post-lockdown stage (April 9–30, 2020), during which anthropogenic activities and transportation in Wuhan gradually recovered. The different lockdown periods and measures are presented in Fig. S17 and Table S2. Here, we discuss the effect of the lockdown on the variations of $PM_{2.5}$ (Fig. 5) and $O_3$ (Fig. 6) concentrations in detail, while the variations of other pollutants are presented in the Supporting Information (Figs. S18–21).

Compared with the corresponding period (Jan 23-Apr 8) of 2015–2019, $PM_{2.5}$ concentrations in Wuhan during the lockdown period in 2020 decreased by 31 μg/m$^3$ (45 %). The S(meteos) of $PM_{2.5}$

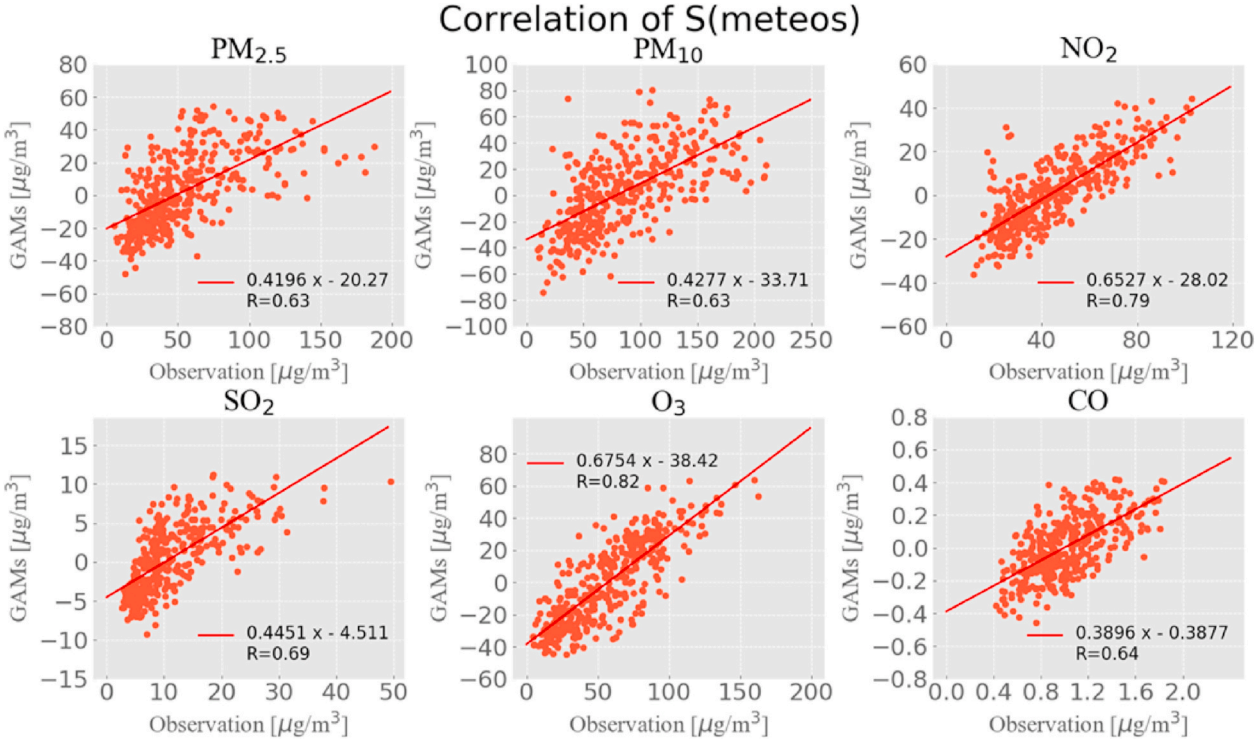


**Fig. 3.** The correlations between observations and S(meteos) data.

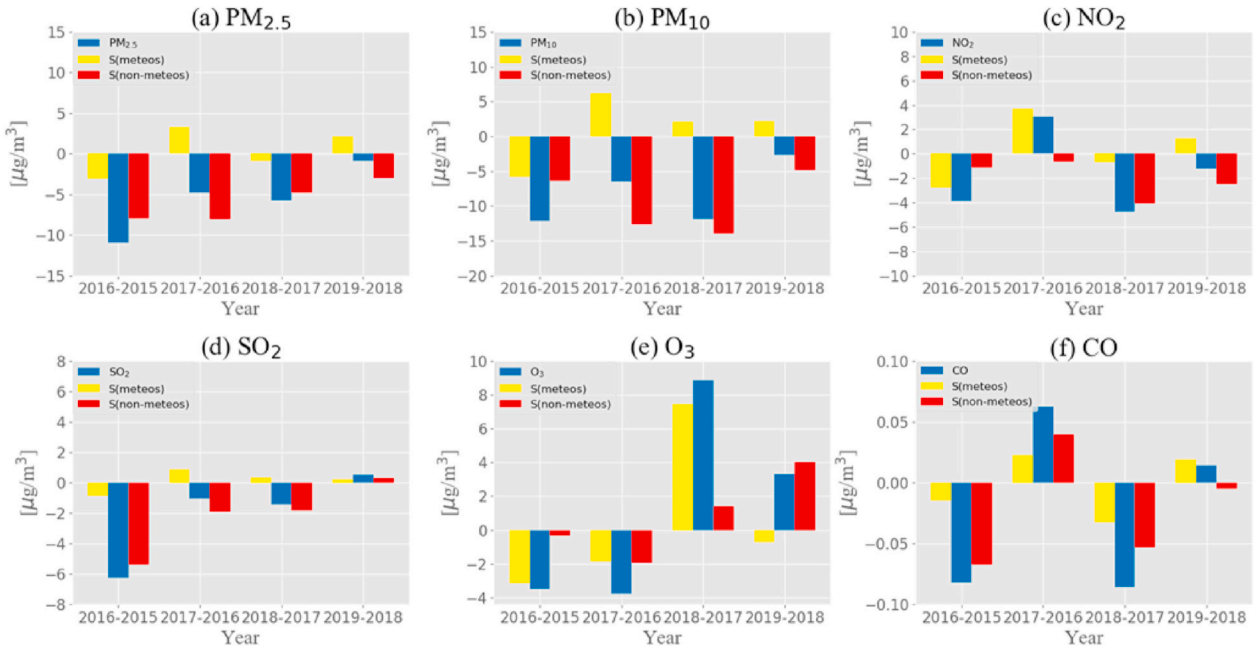


**Fig. 4.** The bar plots of annual variation of pollution and their S(meteos) and S(non-meteos) relative to the averages of those during 2015–2019. (a) $PM_{2.5}$, (b) $PM_{10}$, (c) $NO_2$, (d) $SO_2$, (e) $O_3$, (f) CO.

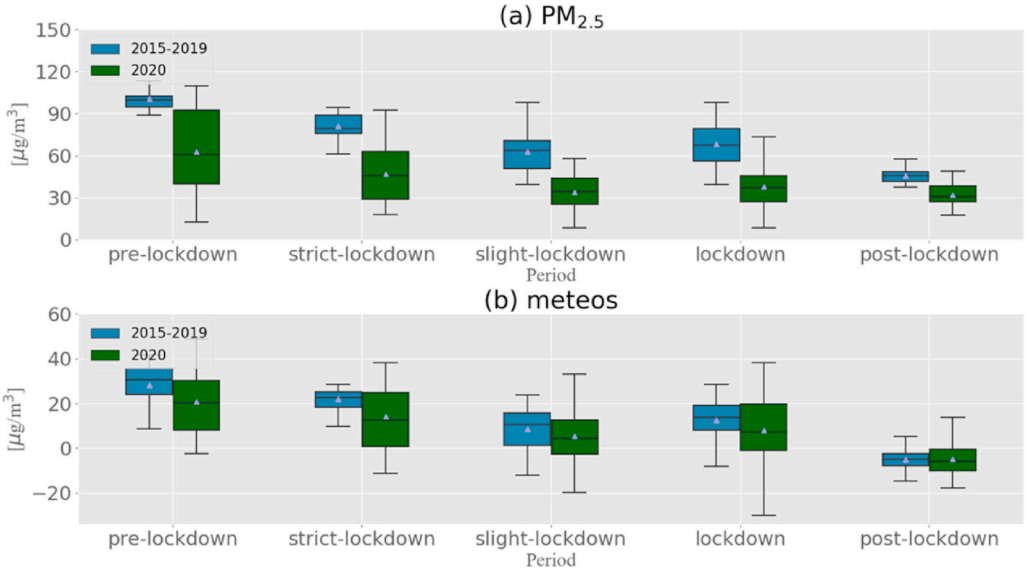


**Fig. 5.** The box plots of (a) and (b) present observed $PM_{2.5}$ and the contribution of meteorological conditions to $PM_{2.5}$ concentrations (S(meteos)) during the pre-lockdown, lockdown including strict-lockdown and slight-lockdown, and post-lockdown periods in 2020, as well as during the corresponding periods in 2015–2019. Each box plot is composed by mean value (blue square points in the middle of boxes), median value (cross in the middle of boxes), 25 % and 75 % value (the lower and upper bounds of each boxplot). The top and bottom extend to a maximum of 1.5 * IQR (interquartile range) from the hinges. (For interpretation of the references to colour in this figure legend, the reader is referred to the Web version of this article.)

decreased by 4.6 μg/m$^3$, which only contributed 15 % to the decline in $PM_{2.5}$. The higher temperature, RH (>60 %), and PBLH caused a decrease of 1.5 μg/m$^3$, 1.4 μg/m$^3$, and 1.1 μg/m$^3$, respectively (Figs. S22 and S23). These results indicate that the reduction of emissions played the critical role in the decrease of $PM_{2.5}$ concentrations during the lockdown period. Although meteorological conditions dominated the day-to-day variations of air pollutants(He et al., 2017), the reduction of anthropogenic emissions played the critical role for pollutant concentrations, from the pre-lockdown to the lockdown period.

From January to April in 2020, manufacturing and construction industry production values had dropped dramatically by −49.3 % and −39.3 % compared with the corresponding period in 2019 in Wuhan (Hubei Provincial Bureau of Statistics, http://tjj.hubei.gov.cn/). Moreover, the energy consumption, especially the consumption of coal decreased significantly because of the large-scale shutdown during the COVID-19 lockdown period, which was an important factor leading to the decrease in particulate matter, and more significantly, its precursors. For the main chemical species of $PM_{2.5}$, Zhang et al.(Zheng et al., 2020) reported that the main components of $PM_{2.5}$ decreased in Wuhan, especially trace elements (0.65 %) and elemental carbon (0.67 %), indicating that primary emissions were reduced due to the lockdown. However, the photochemical reactions involving $O_3$ and OH radicals contribute significantly to $PM_{2.5}$ formation during the lockdown period due to the increase in ozone and this may explain the slight decrease in $PM_{2.5}$ during confinement in comparison with other pollutants like $NO_x$ and $SO_2$ (Sbai et al., 2021).

Moreover, compared with the strict-lockdown stage, $PM_{2.5}$ concentrations during the slight-lockdown stage decreased by 14 μg/m$^3$ (29 %), and the S(meteos) of $PM_{2.5}$ decreased by 10.2 μg/m$^3$, which contributed 73 % to the decline in $PM_{2.5}$. The main reason was increasing of

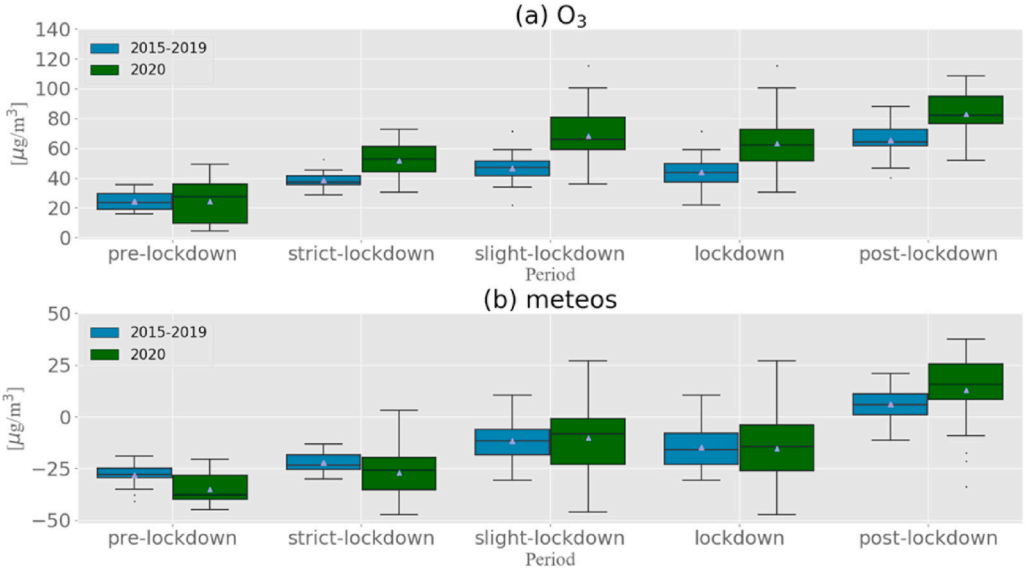


**Fig. 6.** The box plots of (a) and (b) present observed O3 and the contribution of meteorological conditions to O3 concentrations (S(meteos)) during the pre-lockdown, lockdown including strict-lockdown and slight-lockdown, and post-lockdown periods in 2020, as well as during the corresponding periods in 2015–2019. The meanings of the symbols in the box plots are the same as those in Fig. 5.

temperature by 6 °C (Fig. S23), which contributed 11 μg/m$^3$ (Fig. S22). The concentrations of $PM_{2.5}$ were mainly determined by meteorological conditions because anthropogenic emission sources had basically been eliminated in this period. Additionally, during the post-lockdown period, $PM_{2.5}$ concentrations continued to decrease by 5 μg/m$^3$ compared with the lockdown period, in which meteorological conditions caused a decrease of 12 μg/m$^3$. This indicates that although pollution sources such as factories had been reopened, the $PM_{2.5}$ concentrations decreased due to the favorable meteorological conditions during the post-lockdown period.

### 3.4. Variation in $O_3$ during the lockdown period

Although the concentrations of primary pollutants and particulate matter significantly decreased, the average concentration of $O_3$ during the lockdown period in 2020 increased by 19 μg/m$^3$ (43 %) compared with that during the corresponding period in 2015–2019 (Fig. 6(a)). The contribution of S(meteos) decreased by 1.3 μg/m$^3$, which was mainly caused by RH (contributing 1.9 μg/m$^3$) due to increasing of RH (Figs. 6 (b) and S23). Compared with those during the pre-lockdown period in 2020, the $O_3$ concentrations increased by 28 μg/m$^3$ (117 %) with S (meteos) contributing 7.9 μg/m$^3$, accounting for 28 % (Fig. 6(b)), which was mainly caused by RH (contributing 2.3 μg/m$^3$), temperature (contributing 3.3 μg/m$^3$), and PBLH (contributing 2.2 μg/m$^3$) (Figs. S23 and S24). As $O_3$ is a secondary species, its concentrations were affected by several factors, such as the emission of precursors (Jin et al., 2017; Jin and Holloway, 2015), chemical processes (Baertsch-Ritter et al., 2004; Jacob, 2000), and meteorological conditions (Nan et al., 2018; Wu et al., 2008). Meteorological factors could only partially explain the increase in ozone, so that the main reasons for this increase were precursor emissions and chemical process effects.

To further investigate the impact of changes in precursors and their photochemical reactions, we used VCDs of formaldehyde (HCHO) extracted from satellite-based observations to trace the variation of VOCs. The contribution of VOCs to the production of $O_3$ was determined by their total reactivity with OH radicals (Sillman, 1995). HCHO is a short-lived oxidation product of nearly all VOC species, and VOC species with higher OH reactivity tend to produce more HCHO (Valin et al., 2016). HCHO is also produced at high yields during the oxidation of many NMVOC species (Millet et al., 2006) and emitted directly from anthropogenic and biomass burning activities (Akagi et al., 2011; Li et al., 2017b). Jin et al. (2017) and Li et al. (2019b) used the total HCHO column observed by OMI and TROPOMI satellite products to study the influence of VOC on the formation of $O_3$. Based on their approach, HCHO can be used as an indicator of the total reactivity of VOCs to analyze the formation of $O_3$. As NOx in the ambient air exists mainly in the form of $NO_2$, $NO_2$ can be used as an indicator of $NO_x$ (Lin et al., 2010). The results of S(meteos) derived by the GAMs model were used to remove the effect of meteorological factors for CNEMC data to better study the impact of emissions and chemistry reactions on $O_3$. As $O_3$ produced from photochemical reactions would be immediately titrated by fresh NO in the ambient air ($NO + O_3 \rightarrow NO_2 + O_2$) (Lin et al., 1988; Liu et al., 1987; Sillman, 1999), odd oxygen ($O_x = O_3 + NO_2$) was chosen instead of $O_3$ to trace the intensity of photochemical reactions forming $O_3$ (Mazzeo et al., 2005; Tonnesen and Dennis, 2000; Xue et al., 2014). The data for $NO_2$ of CNEMC are consistent with those of the TROPOMI satellite (Fig. S25).

From the pre-lockdown period to the strict-lockdown period, both $NO_2$ and HCHO dropped significantly; however, the decrease in $NO_2$ (by 56 %) was much larger than that of HCHO (by 30 %) (Fig. 7(a), (e)). These reduction percentages were close to those of $NO_x$ and VOCs in eastern China estimated according to the variations of the level of anthropogenic activities (Huang et al., 2021). Nevertheless, $O_x$ showed no significant change, with a slight decrease of 3 μg/m$^3$ for the average value, indicating that the photochemical production of $O_3$ did not changed significantly (Fig. 7 (d)). Furthermore, lower emissions of $NO_x$ would weaken the titration effect of NO and result in a larger accumulation of $O_3$ (Liu et al., 2020). During the strict-lockdown period, the average concentration of $O_3$ was 58 % higher than that during the pre-lockdown period (Fig. 7 (c)). On the basis of the $O_3$–VOCs-$NO_x$ empirical kinetic modeling approach (EKMA) isopleth mapped via WRF-Chem modeling by Huang et al. (2021), $O_3$ production in eastern China (30°N-40°N, 110°E–120°E) in the winter is VOC-limited, and would increase by 40–50 % with an emission decrease of $NO_x$ and VOCs by 43 % and 30 %, which is in good agreement with our observation results. This VOC-limited regime is also certified by the variations of HCHO, $NO_2$, and $O_3$ in 2019. From January to April in 2019, $NO_2$ declined gradually, while HCHO remained stable, which resulted in a slightly decreasing trend for $O_x$ and an increasing trend for $O_3$. Due to the VOC-limited regime for $O_3$ production in the winter in China (Li

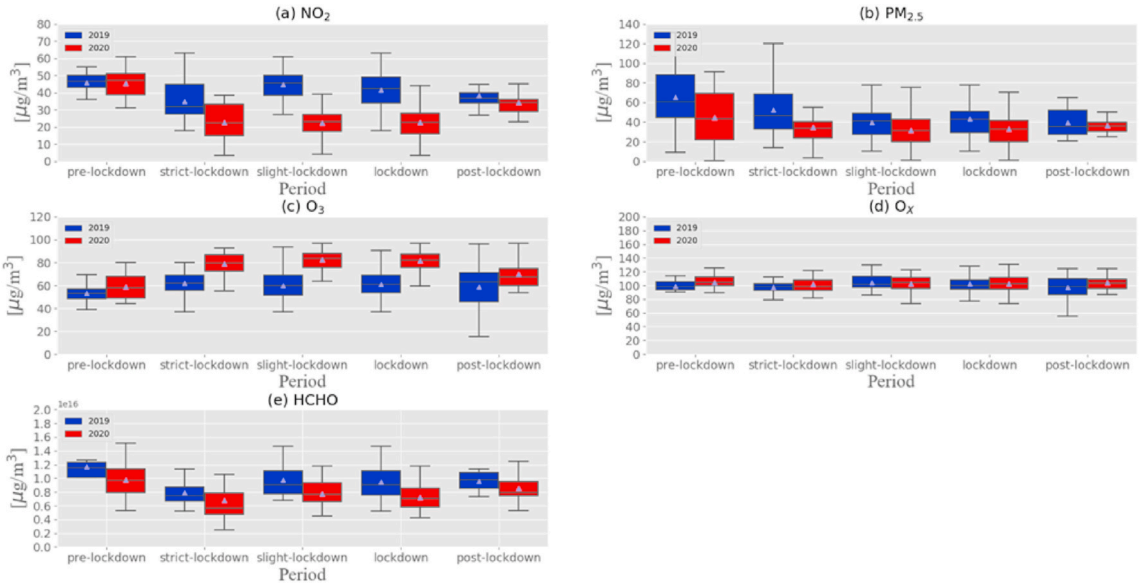


**Fig. 7.** (a) The box plots of $NO_2$ at the surface after the removal of meteorological effects during the pre-lockdown, lockdown including strict-lockdown and slight-lockdown, and post-lockdown periods in 2020. (b) Similar with (a) but for $PM_{2.5}$. (c) Similar with (a) but for $O_3$. (d) Similar with (a) but for $O_x$. (e) Similar with (a) but for HCHO. The meanings of the symbols in the box plots are the same as those in Fig. 1.

et al., 2019b; Xing et al., 2011), $O_3$ concentrations would not decline if $NO_x$ emissions diminished alone, but probably increase due to the weakening of the titration effect of NO (Liu et al., 2020).

Compared with the strict-lockdown period, $NO_2$ concentrations were relatively stable during the slight-lockdown. The titration effect after the strict-lockdown period changed little. However, HCHO, $O_3$, and $O_x$ concentrations in the slight-lockdown period increased slightly, and the means even exceeded those in strict-lockdown period by $1.02 \times 10^{15}$ molecules/$m^2$ (15 %), 4 μg/$m^3$ (5 %), and 2 μg/$m^3$ (2 %), respectively (Fig. 7 (c)–(e)). Thus, owing to the VOC-limited regime, the increased abundance of VOCs versus $NO_x$ caused an accelerated photochemical production of $O_3$, which, combined with a still weakened titration effect by NO, caused a rapid increase in the $O_3$ concentration after the strict-lockdown period.

Compared with the corresponding period in 2019 (1.1–4.30), HCHO concentrations decreased significantly. However, HCHO concentrations during the slight-lockdown and post-lockdown periods were even slightly higher than those during the corresponding period in 2019 (Fig. 7 (e)). Under atmospheric conditions the depletion of ozone by $NO_x$ is more important than its production (Sbai et al., 2021). The titration effect mainly affects the daily depletion of ozone (Anshika et al., 2021; Feng et al., 2019; Kumar et al., 2010; Reddy et al., 2010; Wang et al., 2020). For diurnal variations, the maximum value of $O_x$ appeared at 5 p.m. during all pre-lockdown, lockdown, and post-lockdown periods. Nevertheless, during the pre-lockdown and post-lockdown periods, the maximum value of $O_3$ occurred at 3 p.m. (Fig. S26 (a), (d)), which indicates that titration started before the end of photochemical reactions, and titration consumed $O_3$ generated by photochemical reactions. However, during the strict-lockdown and slight-lockdown periods, the maximum value of $O_3$ occurred at 5 and 4 p.m. (Fig. S26 (b), (c)), respectively. This means that the titration effect was weakened during daytime, and the titration effect could not consume the $O_3$ generated by photochemical reactions during that time, which resulted in a large increase of the concentration of $O_3$. Meanwhile, during all periods, $O_3$ increased from 7 a.m., suggesting that the large reduction in $NO_x$ has no particular effect on $O_3$ production, even though $NO_x$ is also the main source of $O_3$ production (Fig. S26). Accordingly, $O_3$ concentrations during the slight-lockdown and post-lockdown periods in 2020 were above those during the corresponding periods in 2019. In Wuhan, the generation of $O_3$ is controlled by VOCs. Conventional emission reduction measures would result in a sharp reduction of $NO_x$, but the reduction in VOCs was insufficient to reduce $O_3$ concentrations in Wuhan in the winter, even if the measures had been implemented to the limit. To further prevent $O_3$ pollution, more refined and VOC-specific measures should be considered.

## 4. Conclusion

In this study, the significant variations in air pollutants in Wuhan, where the first city implemented lockdown measure during COVID-19 were presented, including $PM_{2.5}$, $PM_{10}$, $NO_2$, $SO_2$, and CO decreased by 45 %, 49 %, 56 %, 39 %, and 18 % compared with the corresponding period in 2015–2019, yet $O_3$ increased by 43 %. We evaluated the meteorological and non-meteorological influence of each pollutant during COVID-19 period using GAMs model. The significant variations in each pollutant are mainly caused by non-meteorological factors (e.g., anthropogenic emissions). The weakening of the titration effect of surface ozone depletion due to the significant reduction emission of $NO_x$ (43 %) was the main cause of the significant increasing of $O_3$. Therefore, we believe that conventional emission reduction ($NO_x$ reduction only) measures may not be sufficient to reduce (or even lead to an increase of) surface $O_3$ concentrations, even if reaching the limit, and VOC-specific measures should also be taken. For the control of $O_3$ pollution, a synergistic control of multiple pollutants including $PM_{2.5}$, $NO_x$ and VOCs should be carried out.

## Author statement

Hao Yin: Conceptualization, Methodology, Software, Validation, Formal analysis, Investigation, Writing-original draft, Visualization. Cheng Liu: Conceptualization, Investigation, Supervision, Funding acquisition, Writing – review & editing. Qihou Hu: Conceptualization, Investigation, Supervision, Funding acquisition, Writing – review & editing. Ting Liu: Conceptualization, Methodology, Software. Shuntian Wang: Formal analysis, Investigation, Visualization. Meng Gao: Conceptualization, Formal analysis, Investigation; Shiqi Xu: Conceptualization, Formal analysis, Investigation; Chengxing Zhang: Methodology; Wenjing Su: Methodology.

## Declaration of competing interest

The authors declare that they have no known competing financial interests or personal relationships that could have appeared to influence the work reported in this paper.

## Acknowledgments

We would like thank to China National Environmental Monitoring Centre for providing free atmospheric environmental monitoring data. Finally, we thank health care workers around the world for their efforts and contributions in the fight against the COVID-19 epidemic, and hope that humanity can overcome the COVID-19 virus soon.

## Appendix A. Supplementary data

Supplementary data to this article can be found online at https://doi.org/10.1016/j.envpol.2021.117899.

## Funding

This work was supported by the National Key Research and Development Program of China (No. 2017YFC0210002, No.2018YFC0213104, No.2016YFC0203302, No.2017YFC0212800 and No.2019YFC0214802), the Chinese Academy of Engineering Grant (2020-ZD-15), the National Natural Science Foundation of China (No. 41722501, No. 51778596, No. 41977184 and No. 41941011), Anhui Science and Technology Major Project (No. 18030801111), the Strategic Priority Research Program of the Chinese Academy of Sciences (No. XDA23020301), the National Key Project for Causes and Control of Heavy Air Pollution (No. DQGG0102 and No. DQGG0205), the Major Projects of High Resolution Earth Observation Systems of National Science and Technology (05- Y30B01-9001-19/20-3).

## References

Akagi, S.K., Yokelson, R.J., Wiedinmyer, C., Alvarado, M.J., Reid, J.S., Karl, T., Crounse, J.D., Wennberg, P.O., 2011. Emission factors for open and domestic biomass burning for use in atmospheric models. Atmos. Chem. Phys. 11, 4039–4072.

Ansari, T.U., Wild, O., Li, J., Yang, T., Xu, W., Sun, Y., Wang, Z., 2019. Effectiveness of short-term air quality emission controls: a high-resolution model study of Beijing during the Asia-Pacific Economic Cooperation (APEC) summit period. Atmos. Chem. Phys. 19 (13) https://doi.org/10.5194/acp-19-8651-2019.

Anshika Kunchala, R.K., Attada, R., Vellore, R.K., Soni, V.K., Mohan, M., Chilukoti, N., 2021. On the understanding of surface ozone variability, its precursors and their associations with atmospheric conditions over the Delhi region. Atmos. Res. 258, 105653.

Atkinson, R., 2000. Atmospheric chemistry of VOCs and NOx. Atmos. Environ. 34, 2063–2101.

Baertsch-Ritter, N., Keller, J., Dommen, J., Prevot, A.S.H., 2004. Effects of various meteorological conditions and spatial emission resolutions on the ozone concentration and ROG/NOx limitation in the Milan area, Atmos. Chem. Phys., 4. In: Atmospheric Chemistry & Physics, vol. 4, pp. 423–438.

Bauwens, M., Compernolle, S., Stavrakou, T., Muller, J.F., van Gent, J., Eskes, H., Levelt, P.F., van der A, R., Veefkind, J.P., Vlietinck, J., Yu, H., Zehner, C., 2020. Impact of coronavirus outbreak on NO(2)Pollution assessed using TROPOMI and OMI observations. Geophys. Res. Lett. 47, 9.

Canton, L., Cabello, M., Barrero, M.A., Orza, J.A., 2015. Categorisation of Air Quality Monitoring Stations by Evaluation of PM10 Variability. Science of the Total Environment.

Cheng, Y.F., Heintzenberg, J., Wehner, B., Wu, Z.J., Su, H., Hu, M., Mao, J.T., 2008. Traffic restrictions in Beijing during the Sino-African Summit 2006: aerosol size distribution and visibility compared to long-term in situ observations. Atmos. Chem. Phys. 8, 7583–7594.

Chinese Government, 2013. Notice of the State Council on Printing and Distributing the Action Plan for the Prevention and Control of Air Pollution. http://www.gov.cn/zhengce/content/2013-09/13/content_4561.htm.

De Veaux, R., 2012. Generalized additive models. Technometrics 34, 225–226.

Elminir, H.K., 2005. Dependence of urban air pollutants on meteorology. Sci. Total Environ. 350, 225–237.

Feng, R., Zheng, H.-j., Zhang, A.-r., Huang, C., Gao, H., Ma, Y.-c., 2019. Unveiling tropospheric ozone by the traditional atmospheric model and machine learning, and their comparison:A case study in hangzhou, China. Environ. Pollut. 252, 366–378.

Gao, M., Carmichael, G.R., Wang, Y., Saide, P.E., Yu, M., Xin, J., Liu, Z., Wang, Z., 2016. Modeling study of the 2010 regional haze event in the North China Plain. Atmos. Chem. Phys. 16, 1673–1691.

Gao, Y., Liu, X., Zhao, C., Zhang, M., 2011. Emission controls versus meteorological conditions in determining aerosol concentrations in Beijing during the 2008 Olympic Games. Atmos. Chem. Phys. 11, 12437–12451.

Han, H., Liu, J., Shu, L., Wang, T., Yuan, H., 2020. Local and synoptic meteorological influences on daily variability in summertime surface ozone in eastern China. Atmos. Chem. Phys. 20, 203–222.

He, J., Gong, S., Yu, Y., Yu, L., Wu, L., Mao, H., Song, C., Zhao, S., Liu, H., Li, X., Li, R., 2017. Air pollution characteristics and their relation to meteorological conditions during 2014–2015 in major Chinese cities. Environ. Pollut. 223, 484–496.

Huang, Q., Wang, T., Chen, P., Huang, X., Zhu, J., Zhuang, B., 2017. Impacts of emission reduction and meteorological conditions on air quality improvement during the 2014 Youth Olympic Games in Nanjing, China. Atmos. Chem. Phys. 17, 13457–13471.

Huang, X., Ding, A., Gao, J., Zheng, B., Zhou, D., Qi, X., Tang, R., Wang, J., Ren, C., Nie, W., Chi, X., Xu, Z., Chen, L., Li, Y., Che, F., Pang, N., Wang, H., Tong, D., Qin, W., Cheng, W., Liu, W., Fu, Q., Liu, B., Chai, F., Davis, S.J., Zhang, Q., He, K., 2021. Enhanced secondary pollution offset reduction of primary emissions during COVID-19 lockdown in China. National Science Review 8.

Jacob, D., Winner, D., 2009. Effect of climate change on air quality. Atmos. Environ. 43.

Jacob, D.J., 2000. Heterogeneous chemistry and tropospheric ozone. Atmos. Environ. 34, 2131–2159.

Jiang, Y.C., Zhao, T.L., Liu, J., Xu, X.D., Tan, C.H., Cheng, X.H., Bi, X.Y., Gan, J.B., You, J. F., Zhao, S.Z., 2015. Why does surface ozone peak before a typhoon landing in southeast China? Atmos. Chem. Phys. 15, 13331–13338.

Jin, X., Fiore, A.M., Murray, L.T., Valin, L.C., Lamsal, L.N., Duncan, B., Folkert Boersma, K., De Smedt, I., Abad, G.G., Chance, K., Tonnesen, G.S., 2017. Evaluating a space-based indicator of surface ozone-NOx-VOC sensitivity over midlatitude source regions and application to decadal trends. J. Geophys. Res.: Atmosphere 122 (10), 410–461, 439.

Jin, X.M., Holloway, T., 2015. Spatial and temporal variability of ozone sensitivity over China observed from the Ozone Monitoring Instrument. Journal of Geophysical Research-Atmospheres 120, 7229–7246.

Johnson, C.E., Collins, W.J., Stevenson, D.S., Derwent, R.G., 1999. Relative roles of climate and emissions changes on future tropospheric oxidant concentrations. J. Geophys. Res.: Atmosphere 104, 18631–18645.

Khoder, M.I., 2002. Atmospheric conversion of sulfur dioxide to particulate sulfate and nitrogen dioxide to particulate nitrate and gaseous nitric acid in an urban area. Chemosphere 49, 675–684.

Kleffmann, J., Wiesen, P., 2005. Heterogeneous conversion of $NO_2$ and NO on $HNO_3$ treated soot surfaces: atmospheric implications. Atmos. Chem. Phys. 5, 77–83.

Kumar, R., Naja, M., Venkataramani, S., Wild, O., 2010. Variations in surface ozone at Nainital: a high-altitude site in the central Himalayas. J. Geophys. Res.: Atmosphere 115.

Lacis, A.A., Hansen, J.E., 1974. Parameterization for absorption OF solar-radiation IN earths atmosphere. J. Atmos. Sci. 31, 118–133.

Le, T., Wang, Y., Liu, L., Yang, J., Yung, Y., Li, G., Seinfeld, J., 2020. Unexpected air pollution with marked emission reductions during the COVID-19 outbreak in China. Science 369, eabb7431.

Leung, D.M., Tai, A.P.K., Mickley, L.J., Moch, J.M., van Donkelaar, A., Shen, L., Martin, R.V., 2018. Synoptic meteorological modes of variability for fine particulate matter (PM2.5) air quality in major metropolitan regions of China. Atmos. Chem. Phys. 18, 6733–6748.

Li, Pin, De, Marco, Alessandra, Feng, Zhaozhong, Anav, Alessandro, Zhou, 2018. Nationwide ground-level ozone measurements in China suggest serious risks to forests. Environ. Pollut. 237, 803–813. https://doi.org/10.1016/j.envpol.2017.11.002.

Li, J., Liao, H., Hu, J., Li, N., 2019a. Severe particulate pollution days in China during 2013–2018 and the associated typical weather patterns in Beijing-Tianjin-Hebei and the Yangtze River Delta regions. Environ. Pollut. 248, 74–81.

Li, K., Jacob, D.J., Liao, H., Shen, L., Zhang, Q., Bates, K.H., 2019b. Anthropogenic drivers of 2013–2017 trends in summer surface ozone in China. Proc. Natl. Acad. Sci. Unit. States Am. 116, 422–427.

Li, L.L., Tan, Q.W., Zhang, Y.H., Feng, M., Qu, Y., An, J.L., Liu, X.G., 2017a. Characteristics and source apportionment of PM2.5 during persistent extreme haze events in Chengdu, southwest China. Environ. Pollut. 230, 718–729.

Li, M., Zhang, Q., Kurokawa, J.I., Woo, J.H., He, K., Lu, Z., Ohara, T., Song, Y., Streets, D. G., Carmichael, G.R., Cheng, Y., Hong, C., Huo, H., Jiang, X., Kang, S., Liu, F., Su, H., Zheng, B., 2017b. MIX: a mosaic Asian anthropogenic emission inventory under the international collaboration framework of the MICS-Asia and HTAP. Atmos. Chem. Phys. 17, 935–963.

Li, P., Wang, L., Guo, P., Yu, S., Mehmood, K., Wang, S., Liu, W., Seinfeld, J.H., Zhang, Y., Wong, D.C., Alapaty, K., Pleim, J., Mathur, R., 2017c. High reduction of ozone and particulate matter during the 2016 G-20 summit in Hangzhou by forced emission controls of industry and traffic. Environ. Chem. Lett. 15, 709–715.

Liang, P., Zhu, T., Fang, Y., Li, Y., Han, Y., Wu, Y., Hu, M., Wang, J., 2017. The role of meteorological conditions and pollution control strategies in reducing air pollution in Beijing during APEC 2014 and Victory Parade 2015. Atmos. Chem. Phys. 17, 13921–13940.

Lin, J., Nielsen, C.P., Zhao, Y., Lei, Y., Liu, Y., McElroy, M.B., 2010. Recent changes in particulate air pollution over China observed from space and the ground: effectiveness of emission control. Environ. Sci. Technol. 44, 7771–7776.

Lin, X., Trainer, M., Liu, S.C., 1988. On the nonlinearity of the tropospheric ozone production. Journal of Geophysical Research-Atmospheres 93, 15879–15888.

Liu, S., Fehsenfeld, F., Parrish, D., Williams, E., Fahey, D., Hübler, G., Murphy, P., 1987. Ozone production in the rural troposphere and the implications for regional and global ozone distribution. J. Geophys. Res. 92, 4191–4207.
Liu, T., Wang, X., Hu, J., Wang, Q., An, J., Gong, K., Sun, J., Li, L., Qin, M., Li, J., Tian, J., Huang, Y., Liao, H., Zhou, M., Hu, Q., Yan, R., Wang, H., Huang, C., 2020. Driving forces of changes in air quality during the COVID-19 lockdown period in the yangtze River Delta region, China. Environ. Sci. Technol. Lett. 7, 779–786.
Lu, X., Hong, J., Zhang, L., Cooper, O., Schultz, M., Xu, X., Tao, W., Gao, M., Zhao, Y., Zhang, Y., 2018. Severe surface ozone pollution in China: a global perspective. Environ. Sci. Technol. 5, 487–494.
Lu, X., Zhang, L., Chen, Y., Zhou, M., Zheng, B., Ke, L., Liu, Y., Lin, J., Fu, T.-M., Zhang, Q., 2019a. Exploring 2016–2017 surface ozone pollution over China: source contributions and meteorological influences. Atmos. Chem. Phys. 19, 8339–8361.
Lu, X., Zhang, L., Shen, L., 2019b. Meteorology and Climate Influences on Tropospheric Ozone: a Review of Natural Sources, Chemistry, and Transport Patterns. Current Pollution Reports.
Mazzeo, N.A., Venegas, L.E., Choren, H., 2005. Analysis of NO, NO2,O-3 and NOx concentrations measured at a green area of Buenos Aires City during wintertime. Atmos. Environ. 39, 3055–3068.
Meng, G., Gufran, B., Shaojie, S., Hongliang, Z., Jianlin, H., Qi, Y., Fengchao, L., Yang, L., Haikun, W., Xiao, L., 2018. The impact of power generation emissions on ambient PM2.5 pollution and human health in China and India. Environ. Int. 121, 250–259.
Millet, D.B., Jacob, D.J., Turquety, S., Hudman, R.C., Wu, S., Fried, A., Walega, J., Heikes, B.G., Blake, D.R., Singh, H.B., Anderson, B.E., Clarke, A.D., 2006. Formaldehyde distribution over North America: implications for satellite retrievals of formaldehyde columns and isoprene emission. J. Geophys. Res.: Atmosphere 111.
Nan, L., Qingyang, H., Jim, G., Alex, G., Jingyi, L., Junji, C., Jun, W., Hong, L., Qiyuan, W., Qiang, Z., 2018. Impacts of biogenic and anthropogenic emissions on summertime ozone formation in the Guanzhong Basin, China. Atmos. Chem. Phys. 18, 7489–7507.
Neftel, A., Spirig, C., Prevot, A.S.H., Furger, M., Stutz, J., Vogel, B., Hjorth, J., 2002. Sensitivity of photooxidant production in the Milan Basin: an overview of results from a EUROTRAC-2 Limitation of Oxidant Production field experiment. Journal of Geophysical Research-Atmospheres 107.
Ordonez, C., H, M., Furger, M., Henne, S., C, H., Staehelin, J., Prevot, A., 2005. Changes of daily surface ozone maxima in Switzerland in all seasons from 1992 to 2002 and discussion of summer 2003. Atmos. Chem. Phys. 5.
Otero, N., Rust, H.W., Butler, T., 2020. Observed changes in the temperature dependence response of surface ozone under NOx reductions. Atmos. Chem. Phys. Discuss. 1–28.
Pearce, J.L., Beringer, J., Nicholls, N., Hyndman, R.J., Tapper, N.J., 2011. Quantifying the influence of local meteorology on air quality using generalized additive models. Atmos. Environ. 45, 1328–1336.
Pendergrass, D., Shen, L., Jacob, D., Mickley, L., 2019. Predicting the impact of climate change on severe wintertime particulate pollution events in beijing using extreme value theory. Geophys. Res. Lett. 46.
Reddy, B.S.K., Kumar, K.R., Balakrishnaiah, G., Gopal, K.R., Reddy, R.R., Ahammed, Y. N., Narasimhulu, K., Reddy, L.S.S., Lal, S., 2010. Observational studies on the variations in surface ozone concentration at Anantapur in southern India. Atmos. Res. 98, 125–139.
Roy, S., Saha, M., Dhar, B., Pandit, S., Nasrin, R., 2021. Geospatial analysis of COVID-19 lockdown effects on air quality in the South and Southeast Asian region. Sci. Total Environ. 756, 144009.
Sbai, S.E., Mejjad, N., Norelyaqine, A., Bentayeb, F., 2021. Air quality change during the COVID-19 pandemic lockdown over the Auvergne-Rhône-Alpes region, France. Air Quality, Atmosphere & Health 14, 617–628.
Shen, L., Jacob, D.J., Liu, X., Huang, G., Wang, T., 2019. An evaluation of the ability of the Ozone Monitoring Instrument (OMI) to observe boundary layer ozone pollution across China: application to 2005-2017 ozone trends. Atmos. Chem. Phys. 19, 6551–6560.
Shi, X., Brasseur, G.P., 2020a. The response in air quality to the reduction of Chinese economic activities during the COVID-19 outbreak. Geophys. Res. Lett. 47, e2020GL088070.
Shi, X.Q., Brasseur, G.P., 2020b. The response in air quality to the reduction of Chinese economic activities during the COVID-19 outbreak. Geophys. Res. Lett. 47, 8.
Sillman, S., 1995. The use of NO y , H2O2, and HNO3 as indicators for ozone-NO x -hydrocarbon sensitivity in urban locations. J. Geophys. Res.: Atmosphere 100, 14175–14188.
Sillman, S., 1999. The relation between ozone, NOx and hydrocarbons in urban and polluted rural environments. Atmos. Environ. 33, 1821–1845.
Sillman, S., Logan, J.A., Wofsy, S.C., 1990. The sensitivity OF ozone to nitrogen-oxides and hydrocarbons IN regional ozone episodes. Journal of Geophysical Research-Atmospheres 95, 1837–1851.
Smedt, I.D., Theys, N., Yu, H., Danckaert, T., Veefkind, P., 2018. Algorithm theoretical baseline for formaldehyde retrievals from S5P TROPOMI and from the QA4ECV project. Atmospheric Measurement Techniques 11, 2395–2426.
Su, T., Li, Z., Kahn, R., 2018. Relationships between the planetary boundary layer height and surface pollutants derived from lidar observations over China: regional pattern and influencing factors. Atmos. Chem. Phys. 18, 15921–15935.
Su, W., Liu, C., Chan, K.L., Hu, Q., Liu, H., Ji, X., Zhu, Y., Liu, T., Zhang, C., Chen, Y., Liu, J., 2020. An Improved TROPOMI Tropospheric HCHO Retrieval over China.
Su, W.J., Liu, C., Hu, Q.H., Fan, G.Q., Xie, Z.Q., Huang, X., Zhang, T.S., Chen, Z.Y., Dong, Y.S., Ji, X.G., Liu, H.R., Wang, Z., Liu, J.G., 2017. Characterization of ozone in the lower troposphere during the 2016 G20 conference in Hangzhou. Sci. Rep. 7.
Tai, A.P.K., Mickley, L.J., Jacob, D.J., 2010. Correlations between fine particulate matter (PM2.5) and meteorological variables in the United States: implications for the sensitivity of PM2.5 to climate change. Atmos. Environ. 44, 3976–3984.
Tonnesen, G.S., Dennis, R.L., 2000. Analysis of radical propagation efficiency to assess ozone sensitivity to hydrocarbons and NOx 1. Local indicators of instantaneous odd oxygen production sensitivity. Journal of Geophysical Research-Atmospheres 105, 9213–9225.
Valin, L.C., Fiore, A.M., Chance, K., González Abad, G., 2016. The role of OH production in interpreting the variability of CH2O columns in the southeast U.S. J. Geophys. Res.: Atmosphere 121, 478–493.
Veefkind, J.P., Aben, I., McMullan, K., Förster, H., de Vries, J., Otter, G., Claas, J., Eskes, H.J., de Haan, J.F., Kleipool, Q., van Weele, M., Hasekamp, O., Hoogeveen, R., Landgraf, J., Snel, R., Tol, P., Ingmann, P., Voors, R., Kruizinga, B., Vink, R., Visser, H., Levelt, P.F., 2012. TROPOMI on the ESA Sentinel-5 Precursor: a GMES mission for global observations of the atmospheric composition for climate, air quality and ozone layer applications. Rem. Sens. Environ. 120, 70–83.
Vu, T.V., Shi, Z., Cheng, J., Zhang, Q., He, K., Wang, S., Harrison, R.M., 2019. Assessing the impact of clean air action on air quality trends in Beijing using a machine learning technique. Atmos. Chem. Phys. 19, 11303–11314.
Wang, G., Zhang, R., Gomez, M.E., Yang, L., Levy Zamora, M., Hu, M., Lin, Y., Peng, J., Guo, S., Meng, J., Li, J., Cheng, C., Hu, T., Ren, Y., Wang, Y., Gao, J., Cao, J., An, Z., Zhou, W., Li, G., Wang, J., Tian, P., Marrero-Ortiz, W., Secrest, J., Du, Z., Zheng, J., Shang, D., Zeng, L., Shao, M., Wang, W., Huang, Y., Wang, Y., Zhu, Y., Li, Y., Hu, J., Pan, B., Cai, L., Cheng, Y., Ji, Y., Zhang, F., Rosenfeld, D., Liss, P.S., Duce, R.A., Kolb, C.E., Molina, M.J., 2016. Persistent sulfate formation from London Fog to Chinese haze. Proc. Natl. Acad. Sci. Unit. States Am. 113, 13630.
Wang, L., Li, M., Yu, S., Chen, X., Li, Z., Zhang, Y., Jiang, L., Xia, Y., Li, J., Liu, W., Li, P., Lichtfouse, E., Rosenfeld, D., Seinfeld, J., 2020. Unexpected rise of ozone in urban and rural areas, and sulfur dioxide in rural areas during the coronavirus city lockdown in Hangzhou, China: implications for air quality. Environ. Chem. Lett. 18.
Wang, Y., Mcelroy, M.B., Boersma, K.F., Eskes, H.J., Veefkind, J.P., 2007. Traffic restrictions associated with the Sino-African summit: reductions of NŌ x detected from space. Geophys. Res. Lett. 34.
Weber, R.O., Prevot, A.S.H., 2002. Climatology of ozone transport from the free troposphere into the boundary layer south of the Alps during North Foehn. Journal of Geophysical Research-Atmospheres 107.
Wood Simon, N., 2004. Stable and efficient multiple smoothing parameter estimation for generalized additive models. J. Am. Stat. Assoc. 99, 673–686.
World Health Organization, 2021. Coronavirus Disease (COVID-19) Pandemic last accessed. https://www.who.int/emergencies/diseases/novel-coronavirus-2019. (Accessed 30 April 2021).
Wu, S., Mickley, L.J., Jacob, D.J., Rind, D., Streets, D.G., 2008. Effects of 2000–2050 changes in climate and emissions on global tropospheric ozone and the policy-relevant background surface ozone in the United States. J. Geophys. Res. 113. https://doi.org/10.1029/2007JD009639.
Wuhan Government, 2021. last accessed. http://tjj.wuhan.gov.cn/. (Accessed 30 April 2021).
Xing, J., Wang, S.X., Jang, C., Zhu, Y., Hao, J.M., 2011. Nonlinear response of ozone to precursor emission changes in China: a modeling study using response surface methodology. Atmos. Chem. Phys. 11, 5027–5044.
Xu, W.Y., Zhao, C.S., Ran, L., Deng, Z.Z., Liu, P.F., Ma, N., Lin, W.L., Xu, X.B., Yan, P., He, X., Yu, J., Liang, W.D., Chen, L.L., 2011. Characteristics of pollutants and their correlation to meteorological conditions at a suburban site in the North China Plain. Atmos. Chem. Phys. 11, 4353–4369.
Xue, L.K., Wang, T., Louie, P.K.K., Luk, C.W.Y., Blake, D.R., Xu, Z., 2014. Increasing external effects negate local efforts to control ozone air pollution: a case study of Hong Kong and implications for other Chinese cities. Environ. Sci. Technol. 48, 10769–10775.
Yang, J., Ji, Z., Kang, S., Zhang, Q., Chen, X., Lee, S.-Y., 2019. Spatiotemporal variations of air pollutants in western China and their relationship to meteorological factors and emission sources. Environ. Pollut. 254.
Yin, H., Sun, Y., Song, Z., Liu, C., Wang, W., Shan, C., Zha, L., 2021. Remote sensing of atmospheric hydrogen fluoride (HF) over hefei, China with ground-based high-resolution fourier transform infrared (FTIR) spectrometry. Rem. Sens. 13.
Yin, H., Sun, Y.W., Liu, C., Lu, X., Smale, D., Blumenstock, T., Nagahama, T., Wang, W., Tian, Y., Hu, Q.H., Shan, C.G., Zhang, H.F., Liu, J.G., 2020. Ground-based FTIR observation of hydrogen chloride (HCl) over Hefei, China, and comparisons with GEOS-Chem model data and other ground-based FTIR stations data. Opt Express 28, 8041–8055.
Yin, H., Sun, Y.W., Liu, C., Zhang, L., Lu, X., Wang, W., Shan, C.G., Hu, Q.H., Tian, Y., Zhang, C.X., Su, W.J., Zhang, H.F., Palm, M.A., Notholt, J., Liu, J.G., 2019. FTIR time series of stratospheric NO2 over Hefei, China, and comparisons with OMI and GEOS-Chem model data. Opt Express 27, A1225–A1240.
Zhang, C., Liu, C., Hu, Q., Cai, Z., Su, W., Xia, C., Zhu, Y., Wang, S., Liu, J., 2019a. Satellite UV-Vis spectroscopy: implications for air quality trends and their driving forces in China during 2005–2017. Light Sci. Appl. 8, 100.
Zhang, F., Wang, Y., Peng, J., Chen, L., Sun, Y., Duan, L., Ge, X., Li, Y., Zhao, J., Liu, C., Zhang, X., Zhang, G., Pan, Y., Wang, Y., Zhang, A.L., Ji, Y., Wang, G., Hu, M., Molina, M.J., Zhang, R., 2020. An unexpected catalyst dominates formation and radiative forcing of regional haze. Proc. Natl. Acad. Sci. Unit. States Am. 117, 3960.
Zhang, Q., Zheng, Y., Tong, D., Shao, M., Wang, S., Zhang, Y., Xu, X., Wang, J., He, H., Liu, W., Ding, Y., Lei, Y., Li, J., Wang, Z., Zhang, X., Wang, Y., Cheng, J., Liu, Y., Shi, Q., Hao, J., 2019b. Drivers of improved PM 2.5 air quality in China from 2013 to 2017. Proc. Natl. Acad. Sci. Unit. States Am. 116, 201907956.
Zhao, W., Tang, G.Q., Yu, H., Yang, Y., Wang, Y.H., Wang, L.L., An, J.L., Gao, W.K., Hu, B., Cheng, M.T., An, X.Q., Li, X., Wang, Y.S., 2019. Evolution of boundary layer ozone in Shijiazhuang, a suburban site on the North China Plain. J. Environ. Sci. 83, 152–160.

Zheng, B., Zhang, Q., Zhang, Y., He, K.B., Wang, K., Zheng, G.J., Duan, F.K., Ma, Y.L., Kimoto, T., 2015. Heterogeneous chemistry: a mechanism missing in current models to explain secondary inorganic aerosol formation during the January 2013 haze episode in North China. Atmos. Chem. Phys. 15, 2031–2049.

Zheng, H., Kong, S., Chen, N., Yan, Y., Qi, S., 2020. Significant Changes in the Chemical Compositions and Sources of PM2.5 in Wuhan since the City Lockdown as COVID-19. Science of the Total Environment, p. 140000.

Zhong, J., Zhang, X., Dong, Y., Wang, Y., Liu, C., Wang, J., Zhang, Y., Che, H., 2018. Feedback effects of boundary-layer meteorological factors on cumulative explosive growth of PM2.5 during winter heavy pollution episodes in Beijing from 2013 to 2016. Atmos. Chem. Phys. 18, 247–258.

Zhu, J., Liao, H., Li, J., 2012. Increases in aerosol concentrations over eastern China due to the decadal-scale weakening of the East Asian summer monsoon. Geophys. Res. Lett. 39.